

# THE STRUCTURE OF A SELF-GRAVITATING PROTOPLANETARY DISK AND ITS IMPLICATIONS TO DIRECT IMAGING OBSERVATIONS

TAKAYUKI MUTO<sup>1</sup>

Department of Earth and Planetary Sciences, Tokyo Institute of Technology,  
2-12-1 Oh-okayama, Meguro-ku, Tokyo, 152-8551, Japan

*ApJ accepted*

## ABSTRACT

We consider the effects of self-gravity on the hydrostatic balance in the vertical direction of a gaseous disk and discuss the possible signature of the self-gravity that may be captured by the direct imaging observations of protoplanetary disks in future. In this paper, we consider a vertically isothermal disk in order to isolate the effects of self-gravity. The specific disk model we consider in this paper is the one with a radial surface density gap, at which the Toomre's  $Q$ -parameter of the disk varies rapidly in the radial direction. We calculate the vertical structure of the disk including the effects of self-gravity. We then calculate the scattered light and the dust thermal emission. We find that if the disk is massive enough and the effects of self-gravity come into play, a weak bump-like structure at the gap edge appears in the near-infrared (NIR) scattered light, while no such bump-like structure is seen in the sub-mm dust continuum image. The appearance of the bump is caused by the variation of the height of the surface in the NIR wavelength. If such bump-like feature is detected in future direct imaging observations, with the combination of sub-mm observations, it will bring us useful information about the physical states of the disk.

*Subject headings:* protoplanetary disks

## 1. INTRODUCTION

Direct imaging observations of protoplanetary disks have been making rapid progress. In the near-infrared (NIR) wavelength, the strategic observation program using Subaru telescope, Subaru Strategic Exploration of Exoplanets and Disks (SEEDS), is now under way (Tamura 2009). Several results to date reveal that disks have diverse structures such as an inner hole, a gap or a ring (Thalmann et al. 2010; Hashimoto et al. 2011). In the submillimeter (sub-mm) wavelength, Atacama Large Millimeter/submillimeter Array (ALMA) is expected to observe disks at a spatial resolution that is comparable to, or better than, NIR wavelength.

Direct imaging observation is useful in probing the detailed structures in the outer disk. For example, a telescope with 0.1 arc-second resolution has an ability to resolve the structure with  $\sim 10$  AU scale if the disk is located at 100 pc. Such a spatial resolution is interesting since 10 AU is comparable with the disk scale height at 100 AU away from the central star. The disk scale height is an important scale in considering the dynamical processes of disks.

From a theoretical point of view, it is important to make a disk model that can be used for the interpretation of direct imaging observations of protoplanetary disks, and discuss what we can derive from the observed structures. Comparing the information from different wavelengths is essentially important in order to reveal the real structure of the observed disks.

In this paper, we investigate the effects of self-gravity on the disk vertical structure in the hydrostatic equilibrium and discuss how the signature of self-gravity appears in the direct imaging observations. We consider

the observations of a disk at NIR wavelength, which mainly observe the scattered light from the upper layer of the disk, and the sub-mm dust continuum observations, which reveal the surface density structure of the disk.

One of the fundamental and important properties of the protoplanetary disk is its mass. The sub-mm dust continuum observation is widely used to estimate the mass of the disk, although it suffers the ambiguity of the dust opacity, which results in at least a factor of two uncertainty in the disk mass. In this paper, we consider the effects of self-gravity on the hydrostatic balance of the disk vertical structure, and discuss how the effects of self-gravity may appear in the direct imaging observations. If there is a feature that reflects the self-gravity, it would give an alternative implication about the disk mass other than the strength of the dust continuum.

In order to isolate the effects of self-gravity in the disk structure, we consider a disk with a simple radial surface density variation, namely, a power-law profile with an axisymmetric gap. The variation of the surface density may be produced by the gravitational perturbation by an embedded planet, turbulence, or other causes, but we do not query the cause of such a structure. The question we address is that how such surface density variations may be observed by direct imaging observations at NIR or sub-mm wavelengths and we look for a feature that is unique to a self-gravitating disk.

There are several works on the modeling of a self-gravitating disk for direct imaging observations, especially in relation to the gravitoturbulence and the resulting planet formation. Narayanan et al. (2006) have performed a detailed calculations of line emission based on the hydrodynamic simulations of gravitational instability by Boss (2001), and have shown that unique features in HCO<sup>+</sup> line may appear close to a forming giant planet. Jang-Condell and Boss (2007) have calcu-

muto@geo.titech.ac.jp  
<sup>1</sup> JSPS Research Fellow

lated the scattered light using the same results of hydrodynamic calculations as Narayanan et al. (2006). They have shown that the vertically integrated surface density and the scattered light have no correlation, since strong turbulence induced by a gravitational instability produces blobs in the upper layer of the disk, and the scattered light is strongly affected by them.

In this paper, we consider a laminar disk where the vertical hydrostatic balance is achieved. Therefore, our model is not useful in a strongly turbulent disk where the Toomre's  $Q$ -parameter (defined in the later section) becomes smaller than  $\sim 1.5 - 2$ , when non-axisymmetric gravitational instability causes the disk to be in a turbulent state (e.g., Mejía et al. (2005); Boley et al. (2006)).

The paper is constructed as follows. In Section 2, we describe the disk model and the methods of calculations. In Section 3, we show the results of calculations. In this section, we also describe the features that appear in the NIR scattered light image and are unique to self-gravitating disks. In Section 4, we discuss the observational implications. Section 5 is for summary and further discussions.

## 2. DISK MODEL

In this section, we describe the basic setup of our model. We consider a model where the outer disk has a gapped structure. We consider a cylindrical coordinate system  $(r, \phi, z)$  with the origin at the central star. As a simple model that features the effects of self-gravity, we assume an axisymmetric disk with a gap:

$$\Sigma(r) = 2.7 f_{\text{enhance}} f_{\text{gap}}(r) \left( \frac{r}{100\text{AU}} \right)^{-1.5} \text{ g/cm}^2, \quad (1)$$

where  $f_{\text{enhance}}$  is a parameter that controls the overall surface density of the disk and  $f_{\text{gap}}(r)$  is a function that determines the shape of the gap. We vary the disk mass by changing  $f_{\text{enhance}}$  from 1 to 8.15, but in the subsequent section, we especially consider the case of  $f_{\text{enhance}} = 1$  and 6.6 as illustrative examples. The case of  $f_{\text{enhance}} = 6.6$  is rather extreme, since the typical  $Q$ -value in this case is close to 2, where turbulence may take place. However, the effects of self-gravity on the vertical structure is prominent in this extreme case. We assume a Gaussian gap profile,

$$f_{\text{gap}}(r) = 1 - \alpha \exp \left[ - \left( \frac{r - r_{\text{gap}}}{\Delta_{\text{gap}}} \right)^2 \right], \quad (2)$$

with  $\alpha = 0.95$ ,  $r_{\text{gap}} = 100\text{AU}$ , and  $\Delta_{\text{gap}} = 30\text{AU}$ . The parameters  $\alpha$ ,  $r_{\text{gap}}$ , and  $\Delta_{\text{gap}}$  parameterize the depth, location and width of the gap, respectively.

In this paper, in order to make the problem simple and tractable, we make a simple assumption for the temperature of the disk. We assume a vertically isothermal disk where the temperature  $T(r)$  is given by

$$T(r) = 30 \left( \frac{r}{100\text{AU}} \right)^{-1/2} \text{ K}. \quad (3)$$

Although we do not question ourselves about the origin of such surface density and temperature structure in detail, we comment here that it is reported that a massive planet emedded in a disk causes a deep gap in the surface density profile, while the temperature does not vary

as significantly as the surface density (D'Angelo et al. 2003).

By varying the overall surface density by  $f_{\text{enhance}}$  while keeping the temperature profile fixed, we vary the disk Toomre's  $Q$ -parameter,  $Q = \Omega c / \pi G \Sigma$ . The  $Q$ -parameter is also varied in the radial direction due to the gap. Figure 1 shows one example of the disk model. In this figure, we show the profile of surface density and  $Q$ -value with  $f_{\text{enhance}} = 1$ .

From the surface density and the temperature profile, we obtain the vertical structure of the disk. We assume that the hydrostatic equilibrium is reached and that the disk is geometrically thin. We solve

$$\frac{dp(z)}{dz} = -\rho(z) \left( \Omega^2 z + \frac{\partial \psi_{\text{d}}}{\partial z} \right), \quad (4)$$

where  $p = c^2 \rho$  is the pressure and  $\Omega(r) = (GM_*/r^3)^{1/2}$  is the Keplerian angular frequency. The sound speed  $c(r)$  is obtained from the temperature profile given by equation (3) by

$$c(r) = 10^5 \left( \frac{T(r)}{300\text{K}} \right)^{1/2} \text{ cm/s}. \quad (5)$$

In equation (4),  $\psi_{\text{d}}$  denotes the gravitational potential of the disk, which is determined by Poisson equation

$$\nabla^2 \psi_{\text{d}} = 4\pi G \rho. \quad (6)$$

We solve equations (4) and (6) iteratively to find a consistent solution. If the variation of the surface density is slow in the radial direction, the local approach by Paczynski (1978) yields a reasonable model. However, in the model presented in this paper, such variation may be rapid due to the presence of the gap, so it is necessary to solve full Poisson equation.

Once we obtain the density structure of the disk, we solve the equations of radiative transfer to obtain the observed image. We consider the thermal emission of the disk and the light from the central star scattered by the disk surface. The former is important in the observations in sub-mm wavelength and the latter is important in the NIR imaging observations. For simplicity, we assume that the dust and gas are well-mixed and the optical properties of the dust particles do not vary in the disk. We also assume that the disk is face-on.

We follow the approach by D'Alessio et al. (1999) in calculating the thermal emission and the scattered light. The thermal emission may be calculated by integrating

$$\frac{dI^{\text{therm}}}{dZ} = -\kappa \rho B(T) \exp[-\tau(Z)], \quad (7)$$

where  $Z$  is the coordinate along the line of sight,  $\kappa$  is the absorption cross section per unit gas mass,  $B(T)$  is the Planck function, and  $\tau$  is the optical depth along the line of sight, which is calculated by

$$\frac{d\tau}{dZ} = -\chi \rho, \quad (8)$$

where  $\chi$  is the total extinction (including absorption and scattering) cross section per unit gas mass. In calculating the scattered light, we assume a single and isotropic scattering. Then, the scattered light can be calculated

by integrating

$$\frac{dI^{\text{scat}}}{dZ} = -\sigma W(r, z) B(T_*) \exp[-\tau_{\text{rad}} - \tau(Z)], \quad (9)$$

along the line of sight. Here,  $\sigma = (\chi - \kappa)\rho$  is the scattering coefficient,  $W(r, z) = 1/4(r^2 + z^2)$  ( $r$  is the radial coordinate and  $z$  is the vertical coordinate) is the geometric dilution factor (e.g., Jang-Condell 2009),  $B(T_*)$  is the blackbody radiation of the central star, and  $\tau_{\text{rad}}$  is the optical depth for the stellar irradiation. In determining  $W(r)$ , we assume that the central star is a point source, which is a reasonable assumption when considering the outer disk.

The opacity of dust particles is one of the major uncertainties in the observational modeling of the disk. Therefore, we use a range of values of the opacity in order to find an opacity-independent signature. We use the total extinction  $\chi$  with  $40 - 200\text{cm}^2/\text{g}$  for the modeling of the NIR observation, and  $1.2 \times 10^{-4} - 6 \times 10^{-3}\text{cm}^2/\text{g}$  for the modeling of sub-mm observation. In the subsequent section, where we describe the effects of self-gravity in detail, we show the results of  $\chi = 100\text{cm}^2/\text{g}$  for NIR observations and  $\chi = 0.003\text{cm}^2/\text{g}$  for sub-mm observations. We use the fixed values of scattering albedo,  $\omega = (\chi - \kappa)/\chi$  for simplicity. We use  $\omega = 0.9$  for the NIR modeling and  $\omega = 10^{-3}$  for the sub-mm modeling.

### 3. SIGNATURE OF A SELF-GRAVITATING DISK

Since we assume that the disk structure is axisymmetric and the disk is face-on, the resulting image is also axisymmetric. Figure 2 shows the examples of the observed radial profile of the relative intensity in NIR wavelength and sub-mm wavelength. The disk brightness is normalized by that at 50AU. The disk with  $f_{\text{enhance}} = 1$  (low-mass disk) and the disk with  $f_{\text{enhance}} = 6.6$  (high-mass disk) are shown. The total extinction coefficient  $\chi$  of the disk is  $100\text{cm}^2/\text{g}$  in NIR and  $0.003\text{cm}^2/\text{g}$  in sub-mm, respectively.

In the sub-mm observation, there is no significant difference in the profile of the disk brightness between the low-mass disk case and the high-mass disk case. This is because in the sub-mm wavelength, the disk is optically thin, and the observed flux is proportional to the disk surface density. In our model, the profile of the surface density is the same in the low-mass and the high-mass case except for the factor  $f_{\text{enhance}}$ . Therefore, the relative intensity profiles are essentially the same in both cases.

In the NIR observation, on the other hand, we see a difference in the radial structure of the relative intensity between the low-mass disk case and the high-mass disk case. In the case of the low-mass disk, the profile of the relative intensity is very similar to that of sub-mm. There is a dark region in the disk around the place where the gap is present. In the case of the high-mass disk, we see that there is a bump in the relative intensity profile at  $\sim 80\text{AU}$  region (indicated by an arrow) beside the dark region around  $\sim 100\text{AU}$ . We also note that there is another bump-like structure outside the gap region. In Figure 2, we see such a structure around  $120 - 140\text{AU}$  region. In the region further away from the central star, we see that the NIR brightness is weakened.

We now focus on the bump-like structure that appears in the NIR profile just inside the gap region (indicated

by an arrow in Figure 2), and we shall show that this structure indeed arises from the effects of self-gravity.

In the left panel of Figure 3, we compare the results of NIR scattered light with and without self-gravity. We use the high-mass disk model with  $f_{\text{enhance}} = 6.6$ . The solid line shows the same calculation with the dashed line in the left panel of Figure 2 and the dashed line in Figure 3 shows the results for the same disk model but the self-gravity is artificially turned off. We see the bump structure around  $\sim 80\text{AU}$  region in the calculations with self-gravity but it is not significant in the calculations without self-gravity.

In order for the bump structure to be seen, it is also necessary to have a gap in the surface density structure. In the right panel of Figure 3, we show the relative intensity profile of the NIR scattered light derived from the calculations with  $f_{\text{enhance}} = 6.6$  but  $f_{\text{gap}}(r) = 1$  everywhere (i.e., no gap). We compare the calculations with and without self-gravity, but there is no significant difference between the two calculations.

As long as the disk is massive enough and there exists a gap structure in the surface density, the bump structure in the NIR profile is always present regardless of the location of the gap or the underlying surface density structure of the disk. Figure 4 shows the NIR profile for the model with  $r_{\text{gap}} = 150\text{AU}$ . In this figure, we compare the results with  $f_{\text{enhance}} = 1$  and  $f_{\text{enhance}} = 6.6$ . We see that there is a bump structure just inside (and also outside) of the gap region. In Figure 5, we show the results of the NIR profile for the disk model with  $\Sigma \propto r^{-1}$ . The disk model is the same with equations (1)-(3) except for the power of the surface density distribution, and we assume  $\alpha = 0.95$ ,  $r_{\text{gap}} = 100\text{AU}$  and  $\Delta_{\text{gap}} = 30\text{AU}$  for the gap profile. We compare the results with  $f_{\text{enhance}} = 1$  and  $f_{\text{enhance}} = 6.6$ . In this model, again, we see a bump-like structure inside and outside of the gap region for  $f_{\text{enhance}} = 6.6$ .

We now discuss the origin of the bump structure in the NIR observation. In the NIR observation, we mainly observe the light from the central star scattered at the surface of the disk. We define the surface of the disk as the place where the optical depth towards the central star,  $\tau_{\text{rad}}$ , becomes unity.

The strength of the scattered light, which is given by equation (9), can be well approximated by using the grazing angle, which is the angle between the incident ray from the central star and the disk surface (see e.g., Inoue et al. 2008; Jang-Condell 2009). The grazing angle can be calculated from the density profile. We have checked that the scattered light profile is indeed well reproduced by the grazing angle times a geometrical factor. Therefore, we discuss the effects of self-gravity on the behavior of the surface of the disk and the grazing angle in the following paragraphs. We note that all the scattered light profiles given so far are calculated by directly integrating equation (9).

We first consider the case where the self-gravity of the disk is negligible. In Appendix, we show explicit calculations of the disk surface and the grazing angle in the case where vertical hydrostatic equilibrium is reached in a non-self-gravitating disk. It is shown that (1) the more the disk material, the higher in the altitude the disk surface is (see equation (A7)), and (2) grazing angle  $\beta$  is

approximately given by

$$\beta \sim h \frac{\rho_0}{\langle \rho_0 \rangle}, \quad (10)$$

where  $h = c/r\Omega$  is the aspect ratio of the disk,  $\rho_0$  is the density at the disk midplane, and  $\langle \rho_0 \rangle$  is the radial average of the midplane density calculated by

$$\langle \rho_0 \rangle = \frac{1}{r} \int dr' \rho_0(r') \quad (11)$$

(see equation (A12)). If there exists a gap in the radial surface density profile and the width of the gap is small compared to the disk scale, the midplane density at the gap location is low while the radially averaged density is not significantly affected by the presence of the gap. Therefore, we conclude that the scattered light traces the surface density profile well, thereby the NIR scattered light is well correlated with sub-mm dust continuum emission. It is possible to see in the left panel of Figure 2 that the location of the dark region in the NIR profile and the location of the gap in the surface density profile are very close each other.

If we include the effects of self-gravity, it acts to pull the disk material towards the disk midplane. Therefore, the disk self-gravity in general lowers the disk surface. Therefore, we expect that the position of the disk surface is maximized at a certain value of  $Q = Q_c$ . Figure 6 shows the disk surface at 50AU (it is well away from the gap region) for various models with  $f_{\text{enhance}}$ . The horizontal axis shows the disk  $Q$ -value at 50AU. It is shown that the disk surface is at the highest place when  $Q = Q_c \sim 5$ . The exact value of  $Q_c$  depends on the place of the disk we consider. For example, we have checked that the value of  $Q_c$  is approximately 3 at 200AU. However, the overall behavior of the location of the disk surface as a function of the disk mass is similar.

Let us now consider what Figure 6 indicates for one particular disk model, in which there is a rapid variation of  $Q$ -parameter in the radial direction. From Figure 6, it is possible to say that if there exists a place where the disk  $Q$ -parameter changes rapidly and crosses  $Q \sim Q_c$ , we expect that the disk surface is at the highest place at such radius. The grazing angle is maximized there, and therefore, the scattered light from such radius is prominent. Figure 7 shows a schematic picture of this. In our disk model, there is a significant change in the disk  $Q$ -value at the location of the gap, and at the edge of the gap, there exists a place where  $Q \sim Q_c$ . Figure 8 compares the profile of the grazing angle in the case of  $f_{\text{enhance}} = 1$  (almost non-self-gravitating) and  $f_{\text{enhance}} = 6.6$  (self-gravitating disk). It is clearly shown that the grazing angle is maximized at the gap inner edge in the case where self-gravity becomes important.

The appearance of the maximum of the grazing angle at the edge of the gap depends on how massive the disk is and to what extent self-gravity effects are important in the vertical structure of the disk. The bump is more enhanced if the disk is more massive. In order to see this, we calculate the strength of the peak at the inner edge of the gap as follows. First, we fit the brightness profile between 35AU and 50AU by power law. We have chosen this region from our data since this region is not significantly affected by the presence of the gap (see Fig-

ure 3). Then, we normalize the profile with the power law profile obtained. Finally, we look for the maximum between 60AU and 100AU from the normalized profile to find the location and the strength of the peak. The choice of 60AU and 100AU is arbitrary, but the point here is that the bump in NIR profile is included in this region.

Figure 9 shows the relation between the peak strength and the averaged  $Q$ -value between 35AU and 50AU. The models with various values of  $f_{\text{enhance}}$  and dust extinction are shown. The different points sharing the same  $Q$ -value correspond to the different values of dust extinction at NIR. It is shown that the smaller the  $Q$ -value, the stronger the peak, and that there is only small range of the  $Q$ -value that can cause the peak strength of 1.15–1.2. There is no significant peak for low-mass disks. For the particular model of  $f_{\text{enhance}} = 6.6$ , which we have discussed in detail in the previous section, the peak strength is of the order of 10%.

In summary, the bump structure at the edge of the gap in the NIR scattered light profile is a characteristic feature arising from the effects of the self-gravity. It is also noted that, in the discussion above, the essential assumption is the vertical hydrostatic equilibrium, rapid variation of the  $Q$ -parameter, and the dominance of the scattered light in NIR observations. We therefore expect that the profile of the surface density is not necessarily a “gap” in order for the bump in the NIR imaging observations to be produced. It is not necessarily axisymmetric, and it can be a “hole” or other such features that exhibit the change in the  $Q$ -parameters, as long as the hydrostatic equilibrium is reached.

#### 4. DISCUSSION: NIR IMAGING OBSERVATIONS OF HIGH-MASS DISKS

We have seen that the bump structure at the gap edge in the NIR observations reflects the fact that the disk self-gravity comes into play in determining the vertical structure of the disk. We now discuss the implications of the results to the observations.

We first note that the peak strength shown in Figure 9 can, in principle, be calculated from the observed relative intensity profile only. From Figure 9, it may be possible to say that if we can detect the peak at the edge of the gap, it may be possible to constrain the disk  $Q$ -value more effectively than by using the sub-mm continuum emission profile alone, which always has an uncertainty of at least a factor of two arising from the uncertainty of the dust parameters.

It is noted, however, that this argument would apply for the disk with a limited range of mass. For low-mass disks (having high  $Q$ -value), the peak is not very significant and it is difficult to constrain the disk mass. This method of estimating the disk mass can be useful for the disk with the  $Q$ -value less than 4 or around. It is also noted that for very high-mass disks with  $Q$ -value less than 2 or around, the disk turbulence is important and the vertical hydrostatic balance may not be reached.

In order to see this self-gravity effects in the actual observations, it is necessary to have a very good sensitivity in the NIR direct imaging observations. As we have seen in Figure 9, it is necessary to detect the peak with the strength of 5 to 10 percent when the disk  $Q$ -value is about 3-4. The typical error of the NIR disk imag-

ing observations is rather difficult to estimate, since it depends on how well the stellar light can be suppressed. In the specific example of the observation of the disk around AB Aur by AEOS telescope (Oppenheimer et al. 2008), Jang-Condell and Kuchner (2010) estimate that the error is typically at the level of  $\sim 20\%$  by fitting the intrinsic azimuthal variation by a certain fitting function and by calculating the rms deviation. It is above the level of the peak strength calculated in this paper. However, in future observations, better suppression of the speckle noise may be made possible.

For the particular model presented in this paper, the required resolution of the telescope can be reached by the current instrument like Subaru. We have checked this by assuming the disk is at 140pc and convolve the NIR profile with the Gaussian with FWHM  $0.04''$ , which is the typical resolution of the Subaru telescope. The resulting image is not much different from the model image.  $0.04''$  at 140pc corresponds to 5.6AU, but the model image varies with the spatial scale of at least 10AU.

We note that although we show that there may be a feature unique to a self-gravitating disk in the NIR scattered light observations, it is essential to compare this feature with the sub-mm observations. Since we can observe only the tenuous surface of the disk in the NIR observations, small surface structure, such as a blob, can also cause the bump-like structure which casts a shadow over the disk (Jang-Condell and Boss 2007). It is therefore necessary to have a sub-mm observation which suggests that the disk is truly massive and there exists a gap in the surface density. The correlation between NIR and sub-mm images must also be checked in order to assure that the hydrostatic balance in the disk vertical direction is reached.

Sub-mm observations are also important in determining how the bump is produced. Another mechanism that may cause the bump-like feature in the NIR scattered light may be localized pressure bumps or a migrating protoplanet. A pressure bump may appear, for example, as a result of baroclinic instability (e.g., Klahr and Boswneheimer 2003). A protoplanet migrating inward in a disk may accumulate gas at the inner edge of a gap and therefore, a bump-like feature may appear (e.g., Rafikov 2002). These processes both act even if the disk mass is low enough and the effects of self-gravity is negligible. Since both processes involve the accumulation of the gaseous materials, such bump structures may also appear in the sub-mm dust continuum emission. It is therefore stressed again that the combination of the sub-mm and the NIR observations is important.

The sub-mm imaging observations should also be used to make a disk model that can be compared with NIR observations. We note that the results presented in Figure 9 are based on the specific model used in this paper. Although we expect that the general trend of the relation between the  $Q$ -value and the peak strength is not very much different if we incorporate other forms of the gap profile or other disk models, it is necessary to make a model that fits with the sub-mm observation data of the surface density profile. It is essential to have at least the same level of spatial resolution between the NIR and sub-mm telescopes.

In summary, if the disk mass is high and the  $Q$ -value is

less than  $\sim 4$ , the effects of self-gravity would come into play in determining the disk vertical structure in hydrostatic equilibrium, and this effect would appear in future NIR direct imaging observations as a detailed structure such as a bump and a gap, if we have sufficient sensitivity. The interpretation of the NIR imaging data would therefore become complicated, especially in high-mass disk case. However, such detailed features may carry important information about the physical states of the disk such as disk mass. The combination between the sub-mm imaging observations and NIR imaging observations are also important in the interpretation of the image.

## 5. SUMMARY AND CAVEATS

In this paper, we have investigated the effects of self-gravity on the vertical structure of a protoplanetary disk with a gap, and discussed the possible signatures of a self-gravitating disk in direct imaging observations. We have seen that the self-gravity of the disk causes a bump feature to appear at the edge of the gap in the NIR imaging observations, especially for the disks with  $Q$ -parameter with  $\sim 3 - 4$ . We have discussed that, although the interpretation of the NIR image would become complicated due to the effects of self-gravity if the disk is very massive, detailed analyses of the morphology of the observed image would provide us useful information about the physical state of the disk.

The combination of the sub-mm and NIR images is important to assure that the disk is truly massive and is in hydrostatic equilibrium in the vertical direction, and to check whether other possible causes of the bump may play a role. Also, since the strength of the dust continuum emission gives a rough estimate of the surface density, it is possible to check the consistency of the model (i.e.,  $f_{\text{enhance}}$  may be estimated both from the peak strength and the strength of the dust continuum emission) if such feature is detected.

Although we have considered a specific disk model with an axisymmetric gap, we expect that the bump structure associated with the gap may be a universal feature in a self-gravitating disk that has a rapid variation in the  $Q$ -value. This feature comes from the fact that the surface of the disk is at the highest altitude in the vertical direction at a certain value of  $Q$ -parameter. The ring geometry is not essential in producing such a bump associated with a gap.

We note that we have assumed the vertical hydrostatic equilibrium, and therefore, our model cannot be used for a turbulent disk. The turbulence induced by the self-gravity is expected to occur when the disk  $Q$ -value becomes less than  $\sim 1.5 - 2$ , and in this case, the structure in the upper layer of the disk may be totally uncorrelated with that at the midplane.

One of the main caveats of the model presented in this paper is the simplification of the temperature structure. Although the assumption of a vertically isothermal disk may not be seriously wrong for the outer disk, the irradiation from the central star can cause a super-heated layer at the surface of the disk (Chiang and Goldreich 1997), which can modify the observed signature in the NIR wavelength. We expect that the surface of the disk may be pumped up by the irradiation from the central star, and the bump structure we have discussed in this paper is more enhanced. Therefore, we expect that the

effects of irradiation may enhance the feature caused by the self-gravity. However, this issue is necessary to be investigated separately.

The author of this paper thanks Munetake Momose,

Akio K. Inoue, and Misato Fukagawa for useful comments. He also thanks the anonymous referee for useful comments that improved the paper. He is supported by Grants-in-Aid for Japan Society for the Promotion of Science (JSPS) Fellows (22-2942).

## APPENDIX

### GRAZING ANGLE

In this Appendix, we show the calculations of the grazing angle between the disk surface and the incident ray in the case of a non-self-gravitating disk. The objective of this section is to show explicitly that the observed NIR flux should be well correlated with the surface density of the disk, which is proportional to the observed sub-mm flux, if the following two conditions are satisfied: (1) the self-gravity of the disk is negligible and (2) the vertical hydrostatic balance is reached.

If the hydrostatic equilibrium in the vertical direction is reached, the density profile of the non-self-gravitating, vertically isothermal disk is given by

$$\rho(r, z) = \rho_0(r) \exp\left[-\frac{z^2}{2H^2}\right], \quad (\text{A1})$$

where  $H$  is the pressure scale height and  $\rho_0(r)$  is the density at the midplane. The midplane density is related to the surface density by

$$\rho_0(r) = \frac{\Sigma(r)}{\sqrt{2}H(r)}. \quad (\text{A2})$$

We first calculate the optical depth,  $\tau_{\text{rad}}$ , between the central star and a point  $(r, z)$  in the disk. Since  $\tau_{\text{rad}}$  is calculated by

$$\frac{d\tau_{\text{rad}}}{dl} = \chi\rho, \quad (\text{A3})$$

where  $l$  is the path connecting between the point  $(r, z)$  and the central star, we have

$$\tau_{\text{rad}}(r, z) = \chi \frac{\sqrt{r^2 + z^2}}{r} \int_{r_{\text{in}}}^r dr' \rho_0(r') \exp\left[-\frac{1}{2h(r')^2} \frac{z^2}{r^2}\right], \quad (\text{A4})$$

where  $h = H/r$  and we have assumed that the central star is a point source situated at the origin.

We first look at the approximate position of the disk surface. We define the disk surface as a place where  $\tau_{\text{rad}} = \tau_s = 1$ . We assume that  $z \ll r$ , which is justified later. The estimate of the order of magnitude of the integration in equation (A4) yields

$$\int dr' \rho_0(r') \exp\left[-\frac{1}{2h(r')^2} \frac{z^2}{r^2}\right], \sim \rho_0 r e^{-z^2/2H^2} \quad (\text{A5})$$

and therefore,  $\tau_{\text{rad}}$  is

$$\tau_{\text{rad}} \sim \chi \rho_0 r e^{-z^2/2H^2}. \quad (\text{A6})$$

Therefore, the surface  $z_s$  of the disk may be calculated by

$$z_s \sim H \sqrt{2 \log\left(\frac{\chi \rho_0 r}{\tau_s}\right)} \sim H \sqrt{2 \log\left(\frac{\chi}{\tau_s} \frac{\Sigma_0}{\sqrt{2}h}\right)}. \quad (\text{A7})$$

If we use  $\Sigma_0 = 10\text{g/cm}^2$ ,  $\chi = 100\text{cm}^2/\text{g}$ ,  $\tau_s = 1$  and  $h = 0.1$ , we have  $z_s \sim 4H$ . Therefore, the disk surface resides at several scale heights above the disk midplane. Since  $H \ll r$  in a protoplanetary disk, this confirms the initial assumption of  $z \ll r$ .

We now look at the grazing angle  $\beta$  between the disk surface and the incident ray. Since  $z_s \ll r$ ,  $\beta$  can be calculated, to a good approximation, by

$$\beta \sim \left. \frac{dz}{dr} \right|_{\text{surf}} - \frac{z_s}{r}, \quad (\text{A8})$$

where  $dz/dr$  should be evaluated along the disk surface,

$$\left. \frac{dz}{dr} \right|_{\text{surf}} = -\frac{\partial \tau_{\text{rad}} / \partial r}{\partial \tau_{\text{rad}} / \partial z} \quad (\text{A9})$$

It is to be noted that from equation (A4),  $\tau_{\text{rad}}(r, z)$  is a function of  $r$  and  $z/r$  only. The grazing angle  $\beta$  is calculated as

$$\beta = - \frac{\sqrt{1 + (z/r)^2} \rho_0(r) \exp[(1/2h^2)(z/r)^2]}{\partial_u [\sqrt{1 + u^2} \int^r dr' \rho_0(r') \exp[-u^2/2h^2]] \Big|_{u=z_s/r}}. \quad (\text{A10})$$

Since  $z_s/r \sim h \ll 1$ , the denominator can be approximated as

$$- \frac{1 + (z_s/r)^2}{z_s/r} \int^r dr' \rho_0(r') \frac{(z_s/r)^2}{h(r')^2} e^{-u^2/2h(r')^2}. \quad (\text{A11})$$

Therefore, the grazing angle is given by

$$\beta \sim \frac{z_s}{r} \frac{\rho_0(r) \exp[-(1/2h^2)(z_s/r)^2]}{r^{-1} \int^r dr' \rho_0(r') (z_s/r h(r'))^2 \exp[-1/2h(r')^2 (z_s/r)^2]}. \quad (\text{A12})$$

Since  $z_s/r \sim h$ , the order of the magnitude of  $\beta$  may be

$$\beta \sim h \frac{\rho_0}{(1/r) \int dr' \rho_0(r')}. \quad (\text{A13})$$

Therefore, we conclude that if there exists a gap in the disk and the gap width is narrow compared to the disk scale, the value of  $\beta$  is almost proportional to the midplane density, which is proportional to the surface density since we assume the hydrostatic equilibrium in a non-self-gravitating disk. Therefore, in this case, the NIR scattered light, whose intensity is proportional to the grazing angle, should be well-correlated with the sub-mm thermal emission, which reflects the profile of surface density.

#### REFERENCES

- Boley, A. C., Mejía, A. C., Durisen, R. H., Cai, K., Pickett, M. K., & D'Alessio, P., *ApJ*, 2006, 651, 517  
 Boss, A. P., *ApJ*, 2001, 563, 367  
 Chiang, E. I., & Goldreich, P., *ApJ*, 1997, 490, 368  
 D'Alessio, P., Calvet, N., Hartmann, L., Lizano, S., & Cantó, J., 1999, *ApJ*, 527, 893  
 D'Angelo, G., Henning, T., & Kley, W., 2003, *ApJ*, 599, 548  
 Hashimoto, J. et al., 2011, *ApJ*, 729, L17  
 Inoue, A. K., Honda, M., Nakamoto, T., & Oka, A., 2008, *PASJ*, 60, 557  
 Jang-Condell, H., 2009, *ApJ*, 700, 820  
 Jang-Condell, H., & Boss, A. P., 2007, *ApJ*, 659, L169  
 Jang-Condell, H., & Kuchner, M. J., 2010, *ApJ*, 714, L142  
 Klahr, H. H., & Bodenheimer, P., 2003, *ApJ*, 582, 869  
 Mejía, A. C., Durisen, R. H., Pickett, M. K., & Cai, K., 2005, *ApJ*, 619, 1098  
 Narayanan, D., Kulesa, C. A., Boss, A., & Walker, C. K., 2006, *ApJ*, 647, 1426  
 Oppenheimer, B. R., et al., *ApJ*, 2008, 679, 1574  
 Paczynski, B., *Acta Astronomica*, 1978, 28, 91  
 Rafikov, R. R., *ApJ*, 2002, 572, 566  
 Tamura, M., 2009, in *AIP Conference Proceedings 1158, EXOPLANETS AND DISKS: THEIR FORMATION AND DIVERSITY*, ed. Usuda, T., Tamura, M., & Ishii, M (New York: AIP), 11  
 Thalmann, C., et al. 2010, *ApJ*, 718, L87

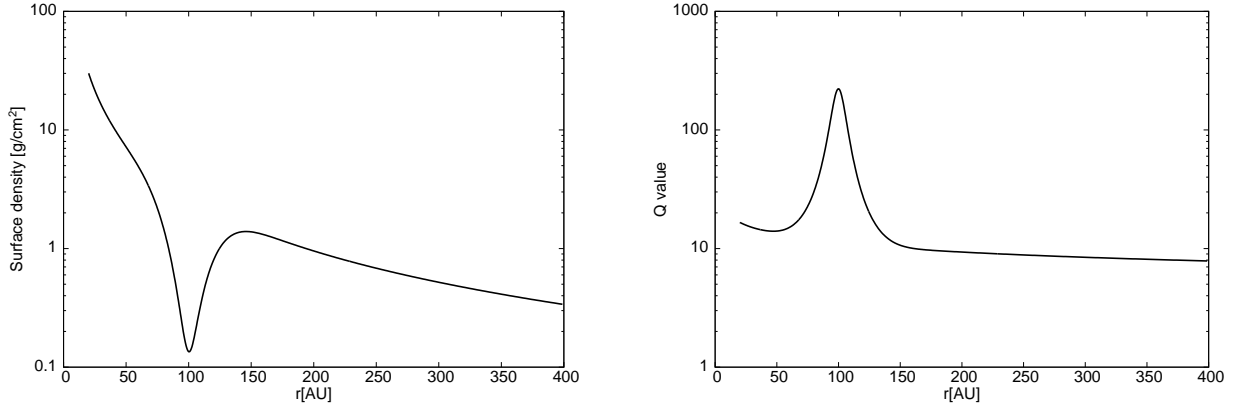


FIG. 1.— An example of the surface density profile and the disk  $Q$ -parameter profile in the model. The left panel shows the surface density of the gas with  $f_{\text{enhance}} = 1$  in equation (1), and the right panel shows the disk  $Q$ -parameter for this model.

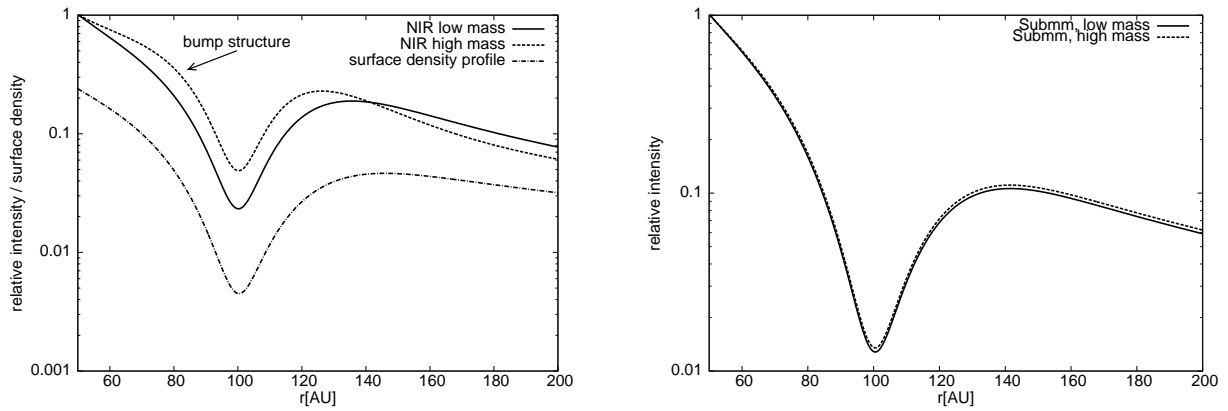


FIG. 2.— The radial profile of NIR observation (left) and sub-mm (right) observation. The surface brightness normalized by that at 50AU is shown. The solid line corresponds to the disk model with  $f_{\text{enhance}} = 1$  (low-mass model) and the dashed line is for  $f_{\text{enhance}} = 6.6$  (high-mass model). The results with extinction  $\chi = 100\text{cm}^2/\text{g}$  (NIR) and  $\chi = 0.003\text{cm}^2/\text{g}$  (sub-mm) is shown. In the left panel, we also show the profile of the surface density in the arbitrary unit by the dot-dashed line. The arrow indicates the “bump” structure which is mainly discussed in this paper.

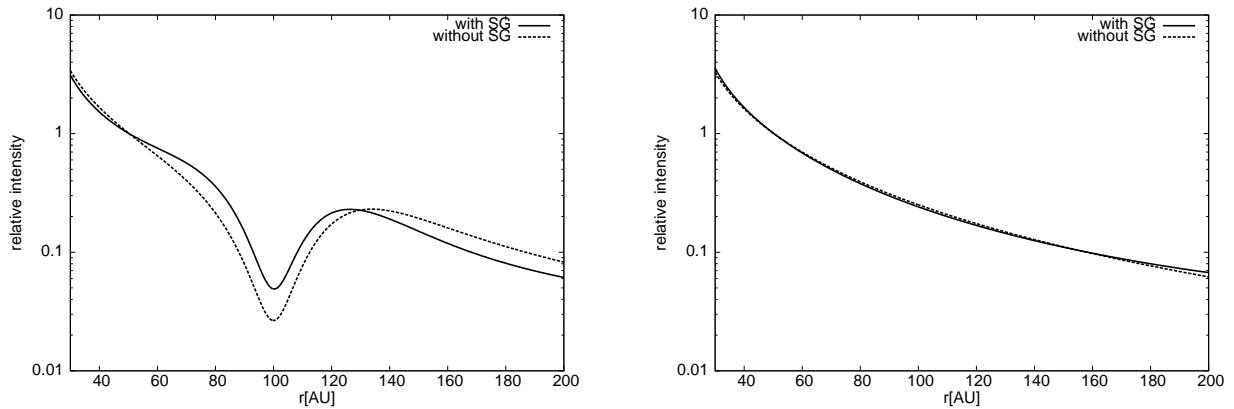


FIG. 3.— Comparison between the calculations with self-gravity and without self-gravity. The left panel shows the disk model with a gap, and the right panel shows the disk model without a gap. The solid line shows the model with self-gravity, and the dashed line is the model without self-gravity. We use the model with  $f_{\text{enhance}} = 6.6$ , which corresponds to the “high-mass model” in Figure 2.

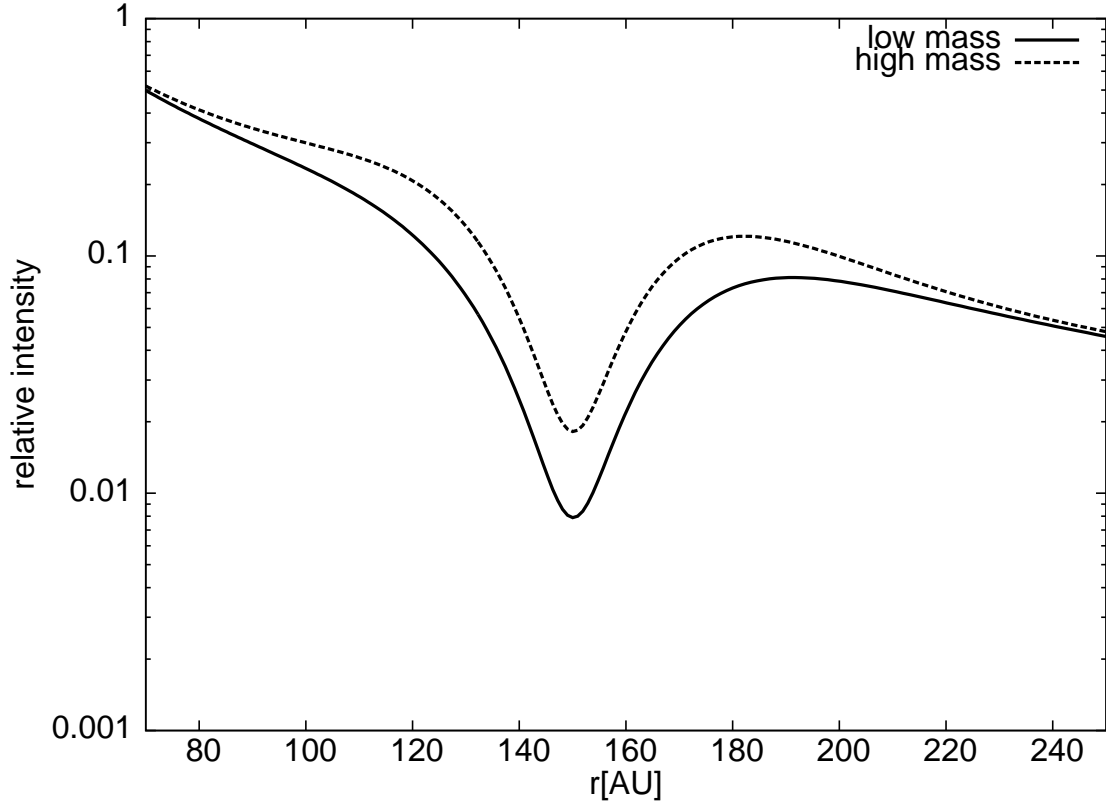


FIG. 4.— The results of NIR profile for the model with the gap at 150AU. The models with  $f_{\text{enhance}} = 1$  (solid line) and with  $f_{\text{enhance}} = 6.6$  (dashed line) are shown. The bump inside and outside the gap region is seen in the case of the high mass disk.

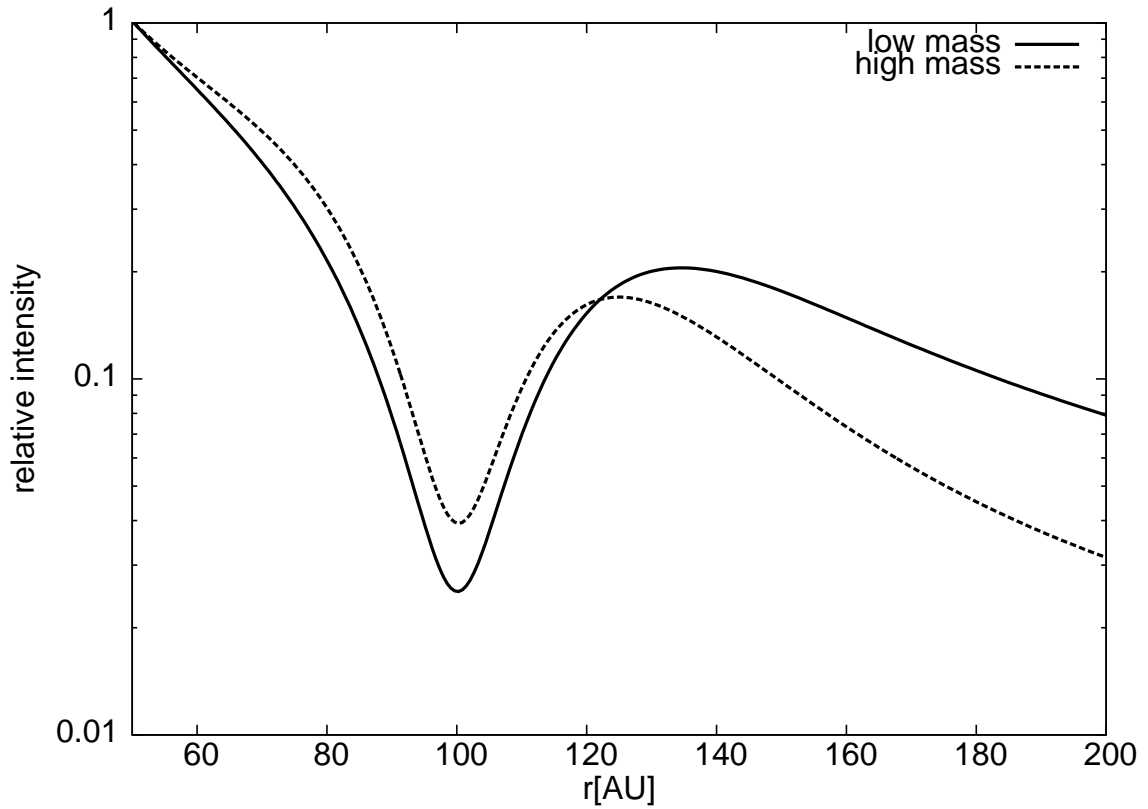


FIG. 5.— The results of NIR profile for the model with the surface density profile of  $\Sigma \propto r^{-1}$ . The models with  $f_{\text{enhance}} = 1$  (solid line) and with  $f_{\text{enhance}} = 6.6$  (dashed line) are shown. The bump inside and the outside the gap region is seen in the case of the high mass disk.

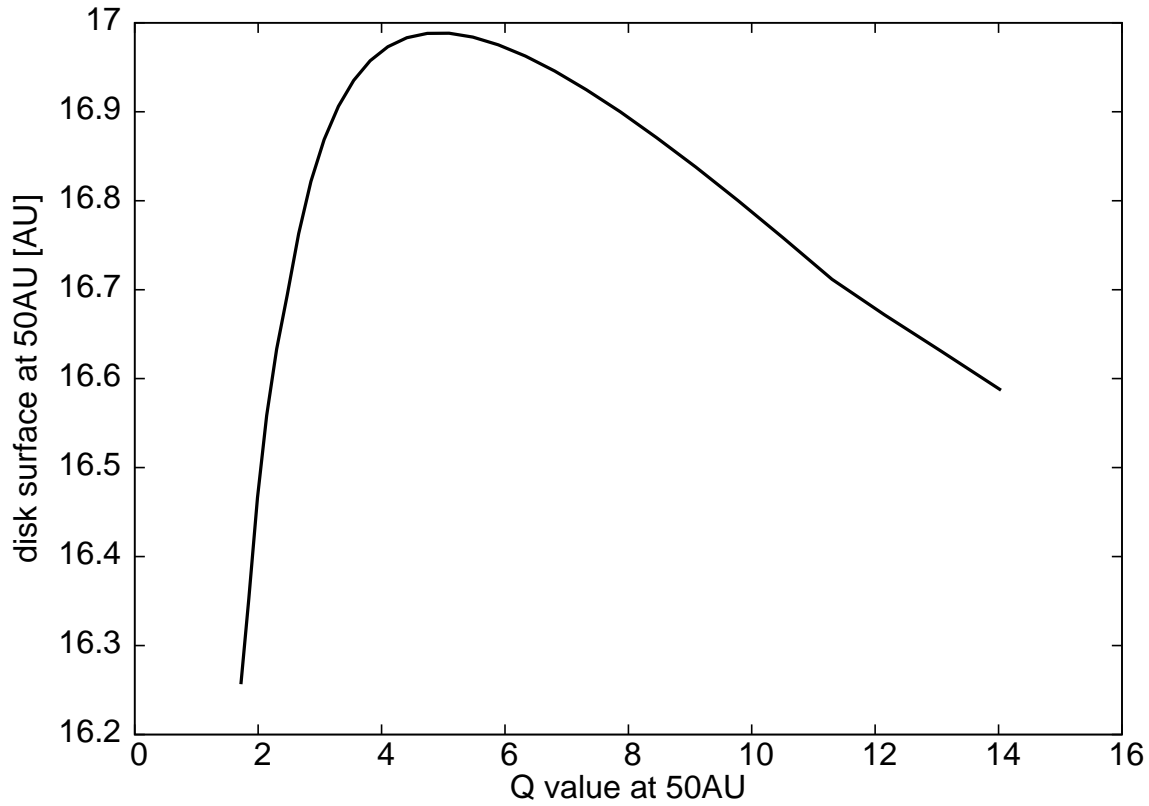


FIG. 6.— The height of the disk surface (in AU) for various disk mass. The surface at 50AU as a function of the  $Q$ -parameter at 50AU is shown. The surface is defined as a place where the optical depth towards the central star is unity. The results with  $\kappa = 100\text{cm}^2/\text{g}$  are shown.

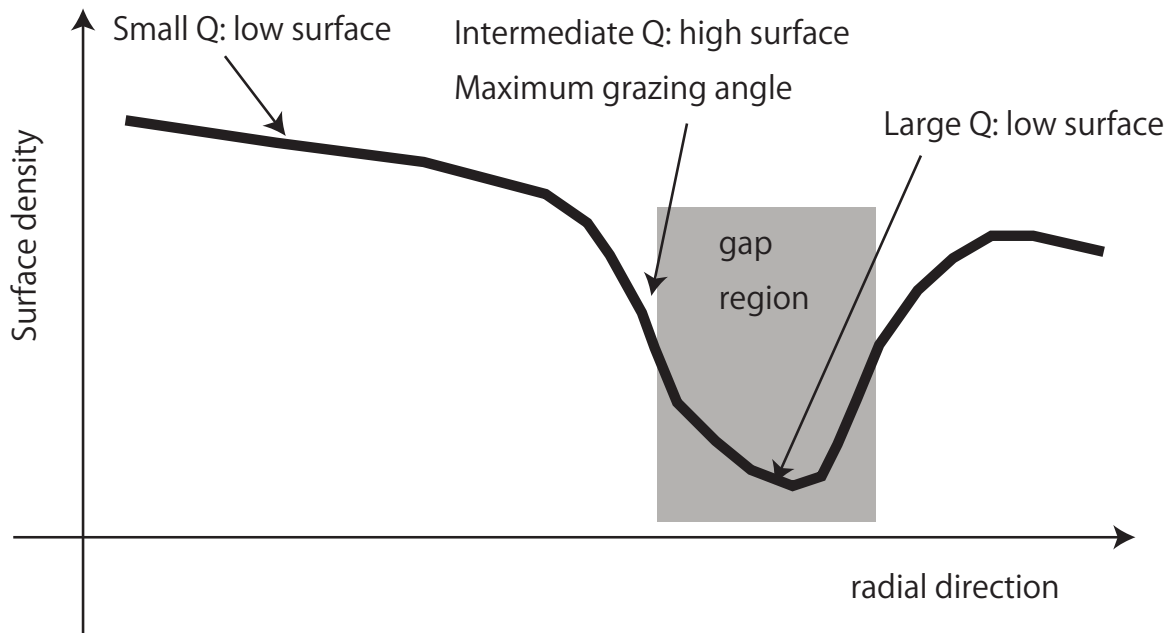


FIG. 7.— Schematic diagram for the origin of bump at the gap edge in NIR observation. In the region where the  $Q$ -value is small, the surface is a relatively lower place because of the effects of the self-gravity. In the region of the gap, the surface is also at a lower place because of the lack of the material. For the intermediate values of  $Q$ , the surface is at the highest place and therefore, the grazing angle is maximum, which leads to the formation of bump in the scattered light.

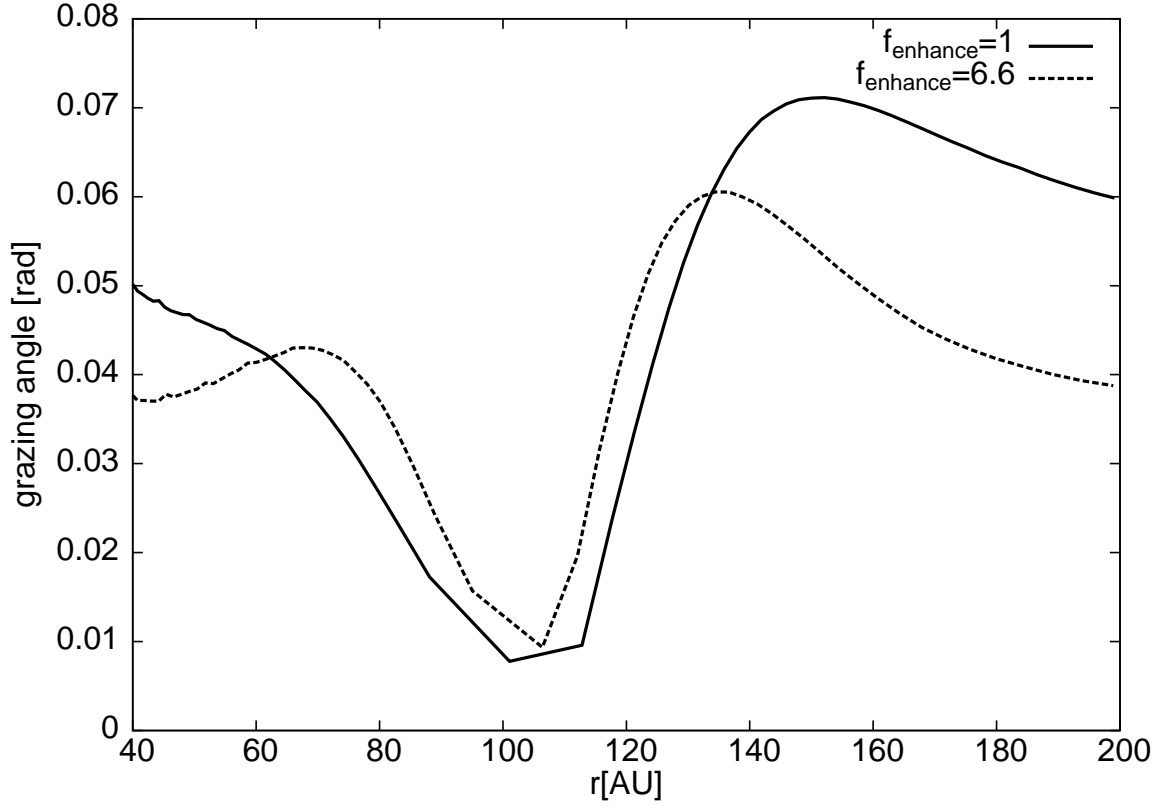


FIG. 8.— The grazing angle (in radian) as a function of radial distance (in AU) in two different  $f_{\text{enhance}}$  parameters. The solid line shows the case of  $f_{\text{enhance}} = 1.0$  and the disk self-gravity is almost negligible. The dashed line shows the case of  $f_{\text{enhance}} = 6.6$ . The effect of self-gravity appears at the gap edge, and there is a maximum of the grazing angle around 70AU region. The results with  $\kappa = 100\text{cm}^2/\text{g}$  are shown.

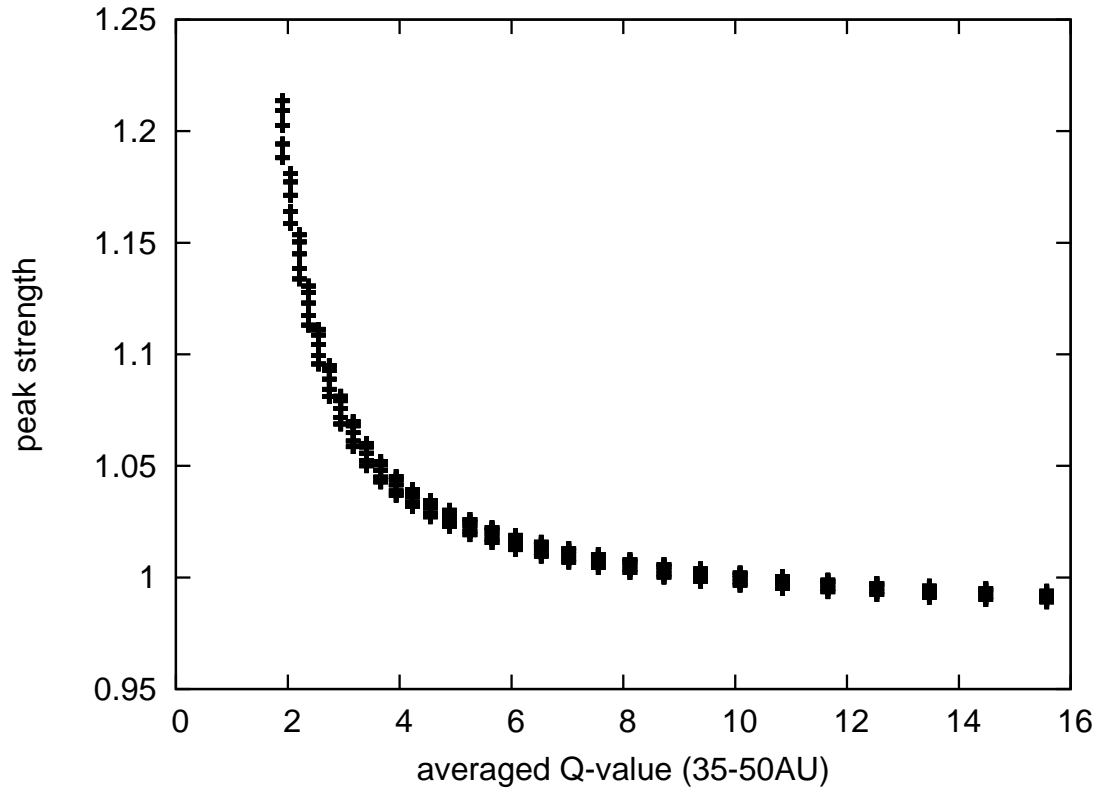


FIG. 9.— The relation between the strength of the peak of the bump in the NIR observations and the  $Q$ -value. The  $Q$ -values are averaged over the radius between 35AU and 50AU. Different points with the same values of  $Q$  correspond to different extinction coefficients  $\chi$  in the NIR wavelength.